International Journal of Bifurcation and Chaos, Vol. 12, No. 1 (2002) 147–157

ASYMPTOTIC ANALYSIS OF A NEW PIECEWISE-LINEAR CHAOTIC SYSTEM

M. A. AZIZ-ALAOUI*
Lab. of Math., Université du Havre, FST, BP 540,
76058 Le Havre cedex, France
aziz@univ-lehavre.fr

GUANRONG CHEN
Department of Electronic Engineering,
City University of Hong Kong, Hong Kong, China
gchen@ee.cityu.edu.hk

Received November 29, 2000; Revised February 23, 2001

Dynamical behavior of a new piecewise-linear continuous-time three-dimensional autonomous chaotic system is studied. System equilibria and their stabilities are discussed. Routes to chaos and bifurcations of the system are demonstrated with various numerical examples, where the chaotic features are justified numerically via computing the system fractal dimensions, Lyapunov exponents and power spectrum.

1. Introduction

A simple yet elegant new chaotic attractor of a three-dimensional continuous-time autonomous system was coined by Chen and Ueta [1999], in the pursuit of anti-controlling chaos [Chen, 1997; Chen & Lai, 1998; Wang & Chen, 1999, 2000]. The new chaotic system reassembles the familiar Lorenz and Rössler systems, but they are nevertheless topologically not equivalent and, in fact, the new system is a *dual system* to the Lorenz system [Lü *et al.*, 2002].

The new system is given by the following closed-form dimensionless equations:

$$\begin{cases} \dfrac{dx}{dt} = a(y - x) \\ \dfrac{dy}{dt} = (c - a)x + cy - xz \\ \dfrac{dz}{dt} = xy - bz, \end{cases} \tag{1}$$

which, with parameters $a = 35$, $b = 3$ and $c = 28$, exhibits the chaotic attractor shown in Fig. 1, which has a prominent 3D feature as compared to the Lorenz attractor.

In recent years, much work has been devoted to building simple electronic circuits, e.g. with piecewise-linear (PWL) functions, to realize chaos in differential systems (see e.g. [Chua, 1990; Baghious & Jarry, 1993; Tokunaga *et al.*, 1989; Tang *et al.*, 2001] and references therein).

We have recently discovered that by replacing the two quadratic-nonlinear terms with PWL terms in Eq. (1), a new chaotic attractor can be generated [Aziz-Alaoui, 2001]. This is further discussed in this paper.

2. The New Chaotic System and Its Basic Properties

More precisely, we study the following modified Chen's system with only PWL nonlinearity

*Author for correspondence.

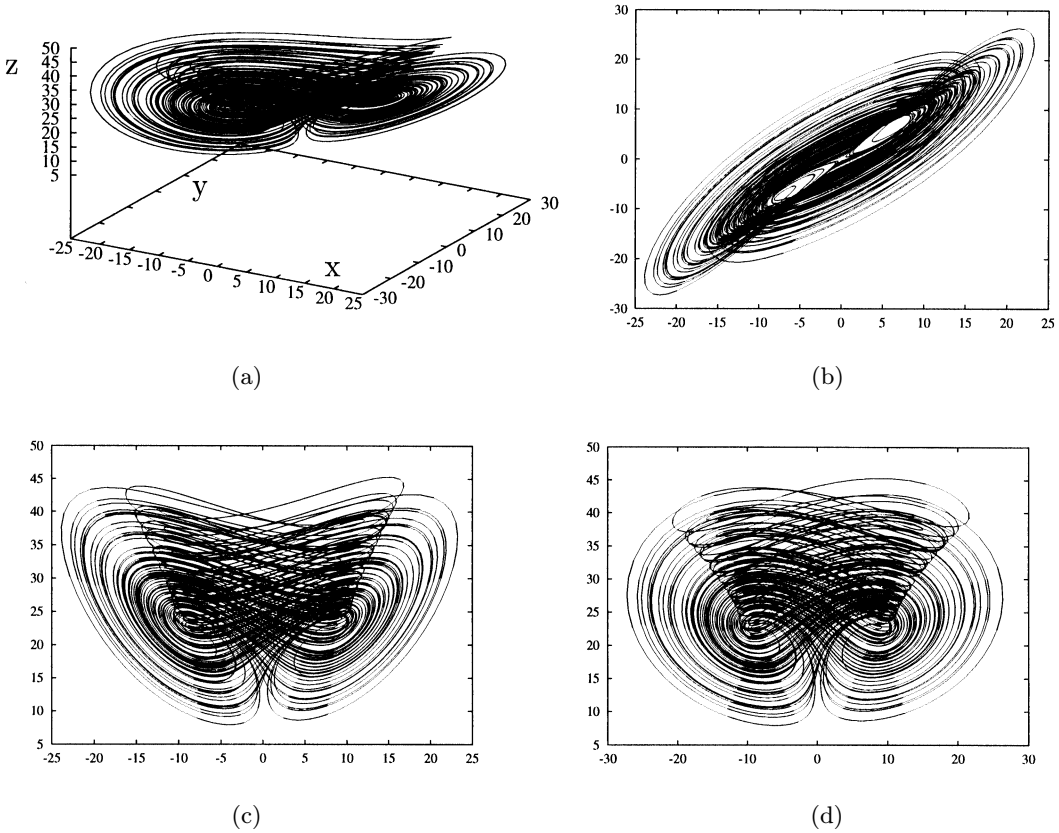

Fig. 1. Chen's chaotic attractor: (a) three-dimensional view, (b) x–y plane projection, (c) x–z plane projection, (d) y–z plane projection.

[Aziz-Alaoui, 2000]:

$$\begin{cases} \dfrac{dx}{dt} = a(y - x) \\ \dfrac{dy}{dt} = \operatorname{sgn}(x)(c - a - z) + cqy \\ \dfrac{dz}{dt} = \operatorname{sgn}(y)x - bz, \end{cases} \tag{2}$$

where $\operatorname{sgn}(\cdot)$ is the standard signum function that gives the sign of its argument and q is a constant parameter.

Clearly, the dynamics of system (2) are no longer governed by the original equation (1).

A detailed study of system (2) for a wide range of parameter values is given in the next section. At this point, it is interesting to compare the new attractor with the familiar Lorenz and Chen attractors, and the graphical comparison is given in Fig. 2.

It should be pointed out that system (2) can be easily implemented by circuitry in the laboratory, as in [Baghious & Jarry, 1993] for another (different but similar) system.

2.1. *Some basic properties*

The new attractor shares several important qualitative properties with both the Lorenz and Chen attractors, respectively. This is further discussed below.

2.1.1. *Symmetry and invariance of the z-axis*

(a) **Symmetry**

The Lorenz and Chen systems both have a natural symmetry under the coordinates transform $(x, y, z) \to (-x, -y, z)$, which persists for all values of the system parameters. It can be easily verified that the new system (2) is also invariant under the same coordinates change. We will use the adjective "symmetric" to refer to those solutions that are taken by the symmetry into themselves. Other solutions will be named "nonsymmetric."

(b) **The z-axis ($x = y = 0$) is invariant**

It is indeed quite obvious that all trajectories that start from the z-axis remain on it and tend towards

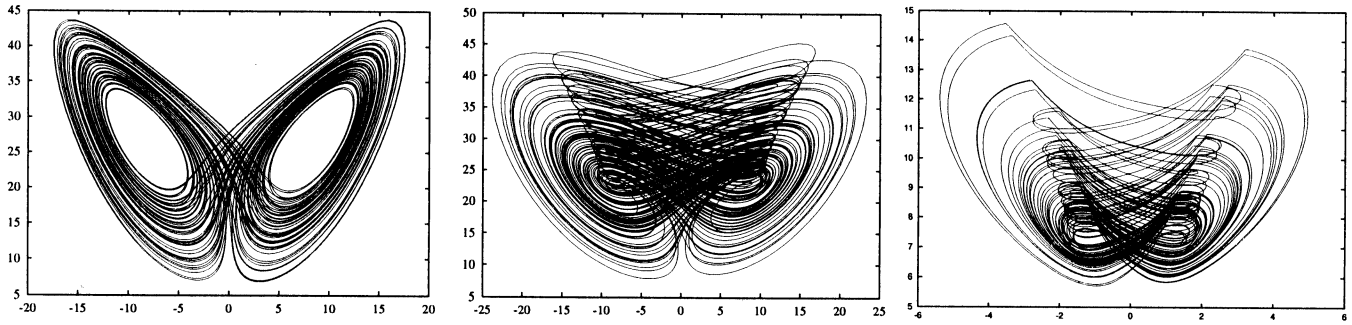

(a) (b) (c)

Fig. 2. Comparison: Projections on the x–z plane of (a) the Lorenz attractor, for $\sigma = 10.0$, $r = 28.0$ and $b = 8.0/3.0$, (b) the Chen attractor, for $a = 35$, $b = 3$ and $c = 28$, (c) the new attractor, for $a = 1.18$, $b = 0.168$, $c = 7.0$ and $q = 0.1$.

the origin, since for such trajectories, $d(x)/dt = d(y)/dt = 0$ and $d(z)/dt = -bz$.

2.1.2. *Dissipativity and the existence of attractor*

Theorem 1. *If $a + b > cq$ then system (2) has a bounded, globally attracting ω-limit set.*

Indeed, the variation of the volume $V(t)$ of a small element $\delta\Omega(t) = \delta x \delta y \delta z$ in the phase space is determined by the divergence of the flow [Lorenz, 1963]:

$$\nabla V = \frac{\partial \dot{x}}{\partial x} + \frac{\partial \dot{y}}{\partial y} + \frac{\partial \dot{z}}{\partial z}\,.$$

From system (2), we get

$$\nabla V = -(a + b - cq)\,,$$

so that, with $a + b > cq$, system (2) is dissipative, with an exponential contraction rate:

$$\delta\Omega(t) = e^{-(a+b-cq)}\,,$$

for the volume element $\delta\Omega(t) = \delta x \delta y \delta z$. That is, a volume element V_0 is contracted by the flow into a volume element $V_0 e^{-(a+b-cq)t}$ in time t.

In other words, each volume containing the system trajectory shrinks to zero as $t \to \infty$ at an exponential rate $-(a+b-cq)$, which is independant of x, y and z. Thus, all trajectories are ultimately confined to a specific subset having zero volume and the asymptotic motion settles onto an attractor. This has been confirmed by our computer simulations (see the next section).

2.2. *Equilibria: Existence and stability*

We now turn to determine the equilibria of system (2) and their types of stability in the sense of Lyapunov.

Due to the nature of the nonlinearities, namely, $\mathrm{sgn}(x)(c-a-z)$ and $\mathrm{sgn}(y)x$, the phase space can be divided into four piecewise-linear regions denoted as D_i, $i \in \{1, \ldots, 4\}$, according to the signs of x and y. In each of these regions, the system becomes linear and one can even obtain its explicit solution formulas. In each of the four regions, there exists a "symmetric" point $P^-(-x, -y, z)$ for each equilibrium point $P^+(x, y, z)$, due to the symmetry of the vector field (recall the invariance under the transform $(x, y, z) \to (-x, -y, z)$).

The equilibria of system (2) can be easily found by solving the three equations $\dot{x} = \dot{y} = \dot{z} = 0$, which lead to

$$a(y - x) = 0\,,$$

$$\mathrm{sgn}(x)(c - a - z) + cqy = 0\,,$$

and

$$\mathrm{sgn}(y)x - bz = 0\,.$$

We thus obtain, in addition to the origin, two "symmetric" equilibria:

$$E_+ = (b\overline{z}, b\overline{z}, \overline{z}) \quad \text{and} \quad E_- = (-b\overline{z}, -b\overline{z}, \overline{z})\,, \tag{3}$$

where

$$\overline{z} = \frac{a - c}{cqb - 1}\,. \tag{4}$$

Let us now study their stability, i.e. the nature of the eigenspaces presented in the neighborhood of each equilibrium.

Note that this system is piecewise-linear, and linear in each region D_i, where the eigenvalues are all constant. Thus, in each region, the associated Jacobian J is constant so that no local approximation is needed to determine it. This is the essential advantage of piecewise-linear systems [Aziz-Alaoui, 1999].

To study the stability of $E_\pm$ and the dynamics near $E_\pm$, which is locally driven by the corresponding linearized system on $E_\pm$, we compute the Jacobian $J_\pm$, evaluated at these equilibria, as follows:

$$J_\pm = \begin{pmatrix} -a & a & 0 \\ 0 & cq & -s_\pm \\ s_\pm & 0 & -b \end{pmatrix}, \tag{5}$$

where $s_\pm = \mathrm{sgn}(x)$.

The eigenvalues are the solutions of the characteristic cubic equation:

$$\Pi(\lambda) = \lambda^3 + A\lambda^2 + B\lambda + C = 0\,, \tag{6}$$

where

$$\begin{cases} A = a + b - cq, \\ B = ab - acq - bcq, \\ C = a(1 - bcq). \end{cases} \tag{7}$$

As for each equilibrium in $x = y$, the equation above does not depend on $s_\pm$; therefore, the Jacobians associated with both equilibria are equal.

The Routh–Hurwitz conditions lead to the conclusion that the real parts of the roots λ are negative if and only if $A > 0$, $C > 0$ and $AB - C > 0$.

In summary, we have proved the following result.

Proposition 2. *The equilibria $E_\pm$ of system (2) have the same stability.*

Actually, we can determine the exact values of the eigenvalues by setting $\lambda = \omega + \Lambda$ in Eq. (6), with $\omega = -(A/3)$. This yields

$$\Pi(\Lambda) = \Lambda^3 + P\Lambda + Q\,,$$

where $P = -(A^2/3) + B$ and $Q = (2A^3/27) - (AB/3) + C$.

This third-order polynomial in Λ can be solved by using the Cardan formula, whereby we set $\Delta = 4P^3 + 27Q^2$, resulting in the following:

(i) If $\Delta > 0$, there is a unique real eigenvalue:

$$\begin{aligned} \lambda_R &= \omega + \Lambda_R \\ &= -\frac{A}{3} + \left(-\frac{Q}{2} + \sqrt{\frac{Q^2}{4} + \frac{P^3}{27}} \right)^{1/3} \\ &\quad + \left(-\frac{Q}{2} - \sqrt{\frac{Q^2}{4} + \frac{P^3}{27}} \right)^{1/3}, \end{aligned} \tag{8}$$

along with two complex conjugate eigenvalues:

$$\begin{aligned} (\lambda_C)^\pm &= \omega + (\Lambda_C)^\pm \\ &= -\frac{A}{3} - \frac{\Lambda_R}{2} \pm \frac{i}{2}\sqrt{4P + 3(\Lambda_R)^2}\,. \end{aligned}$$

(ii) If $\Delta < 0$, the system has three real and distinct eigenvalues:

$$\lambda_1 = -\frac{A}{3} + 2\sqrt{-\frac{P}{3}}\,\sin\left(\frac{\theta}{3}\right),$$

$$\lambda_2 = -\frac{A}{3} + 2\sqrt{-\frac{P}{3}}\,\sin\left(\frac{2\pi + \theta}{3}\right),$$

$$\lambda_3 = -\frac{A}{3} + 2\sqrt{-\frac{P}{3}}\,\sin\left(\frac{4\pi + \theta}{3}\right),$$

where

$$\theta = \arcsin\left(\sqrt{\frac{-27Q^2}{4P^3}}\right) \in [0,\, \pi]\,.$$

The case where $\Delta = 0$ corresponds to a measure-zero set of parameters. So, by a slight perturbation of parameters, without changing the behavior of the system, a system belonging to one of the two other cases is obtained.

Consequently, for the parameter values given by Eq. (9) and for $a = 1.18$, the system has the strange attractor shown in Figs. 2(c) and 3. In this case, the equilibria are:

$$E_+(1.114,\, 1.114,\, 6.6)$$

and

$$E_-(-1.114,\, -1.114,\, 6.6)\,.$$

The eigenvalues corresponding to the linearized vector field are:

$$\lambda_R = -1.5567 \quad \text{and} \quad \lambda_C^\pm = 0.454 \pm 0.68\,i\,.$$

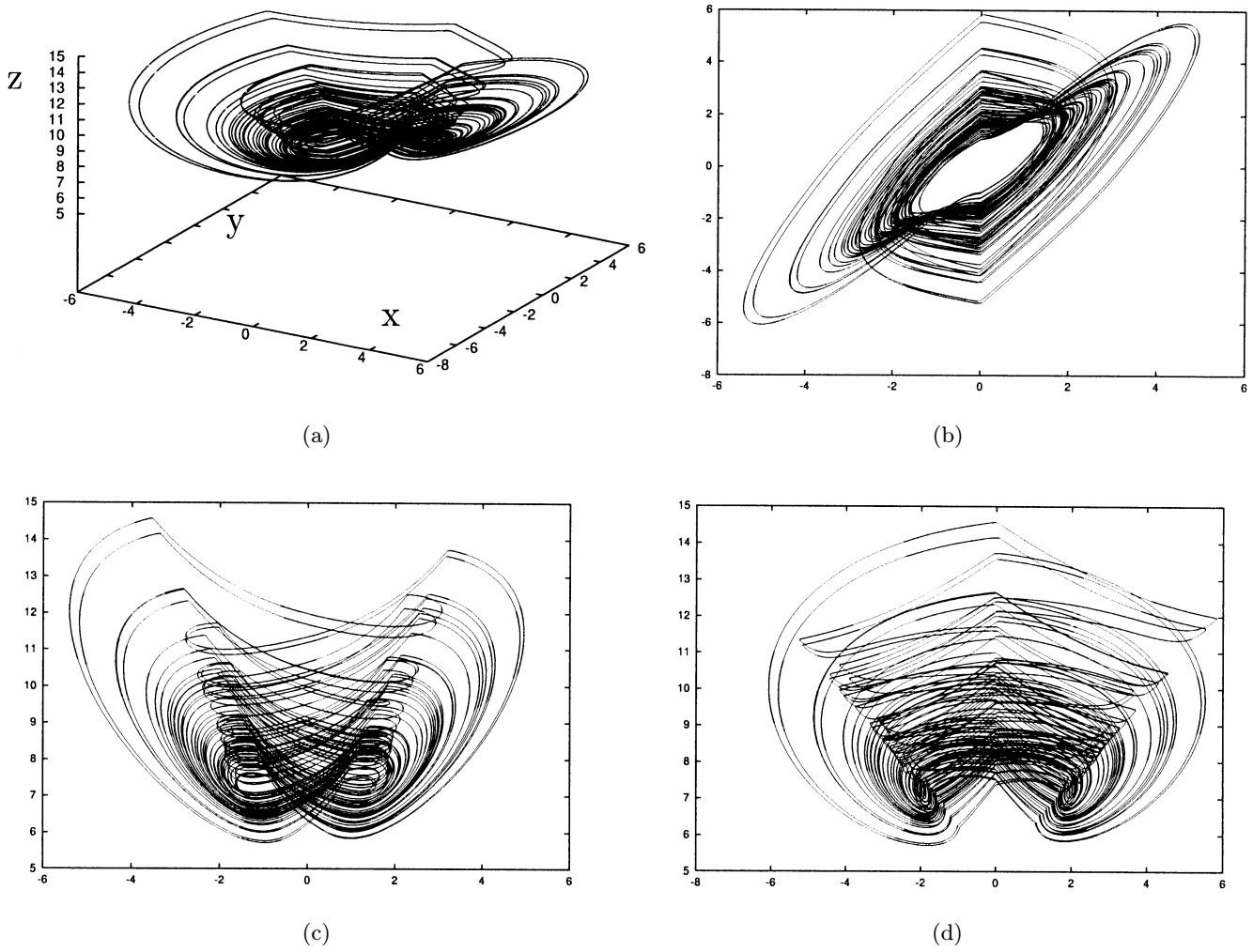

Fig. 3. The chaotic attractor, for the set of parameters specified by Eq. (9) and for $a = 1.18$, the shape of the attractor in the (a) x–y–z space, (b) x–y plane, (c) x–z plane, (d) y–z plane.

Thus, locally, there exit two conjugate complex eigenvalues, $\lambda_C^{\pm}$, and a real eigenvalue, λ_R, where λ_R and $\mathcal{R}e(\lambda_C^{\pm})$ have different signs. Hence, equilibria $E_{\pm}$ are not stable; they are attracting in one direction but repelling in the other two directions.

3. Numerical Investigations

To provide some numerical evidence for the chaotic behavior of system (2), we present various numerical results here to show the chaoticity, including its sensitive dependence on initial conditions, fractal structure, bifurcation diagrams, and Lyapunov exponents.

Throughout, we assume that all parameters of the system are positive and, unless otherwise specified, we fix

$$b = 0.16875\,, \quad c = 7.0\,, \quad q = 0.1\,, \tag{9}$$

and assume

$$c > a\,. \tag{10}$$

Parameter a plays a key role in parameter control below.

For these parameter values, system (2) has the chaotic attractor as shown in detail in Fig. 3.

3.1. *Sensitive dependence on initial conditions and the power spectrum*

To demonstrate the sensitivity to intial conditions of system (2), we compute two orbits with initial

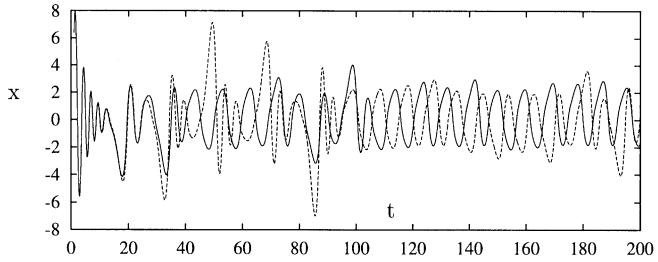

Fig. 4. Sensitive dependence on initial conditions: x-coordinates of the two orbits, for system (2), plotted against the time, with $a = 1.18$; the x-coordinates of initial conditions differ by 0.0001, the other coordinates are kept equal.

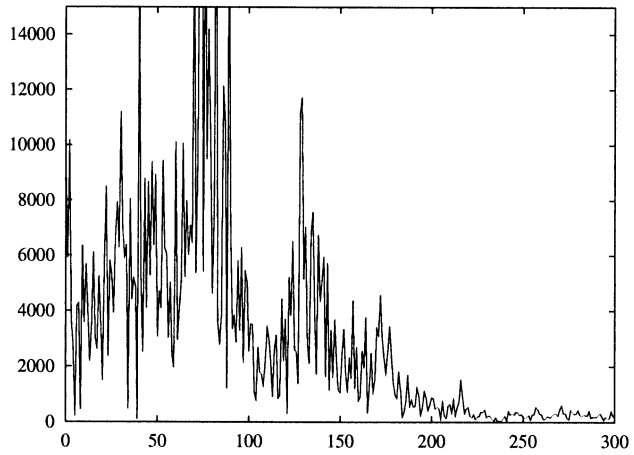

Fig. 5. Power spectrum of the time series $x(t)$, where $a = 1.18$.

points (x_0, y_0, z_0) and $(x_0 + 0.0001, y_0, z_0)$, respectively. The results are shown in Fig. 4. At the beginning, the time series are undistinguishable; but after a number of iterations, the difference between them builds up rapidly.

On the other hand, the aperiodicity of the attractors can be seen from the calculation of the power spectrum of the time series. Here, we have chosen the x-component for demonstration. Figure 5 shows the power spectrum, which was calculated for a very long time series using the algorithm provided by Cooley and Tukey [1965].

From Fig. 5, it seems obvious that the attractor is aperiodic and the power spectrum of orbit $x(t)$ exhibits a continuous broadband feature. It contains a dominant discrete peak at a low frequency that is due to the presence of a limit cycle. This noise-like spectrum is an essential characteristic of chaotic systems.

3.2. *Fractal dimension and Lyapunov exponents*

Strange attractors are typically characterized by fractal dimensions. The correlation dimension is obtained by considering the correlation between "random" points on a chaotic attractor. The computational method used here is taken from [Grassberger & Procaccia, 1983], where the dimension is defined by

$$d = \lim_{\varepsilon \to 0} \frac{\ln(C_i(\varepsilon))}{-\ln \varepsilon}$$

with

$$C_i(\varepsilon) = \frac{1}{N} \{\#\{M_i M_j \in S_N \times S_N : \|M_i M_j\| < \varepsilon\}\},$$

where # indicates the number of points of a set and S_N denotes a set of N points on the attractor, both obtained from a trajectory.

We have numerically found that $d_c = 2.047$ for system (2); this value gives evidence of its fractal structure.

Finally in this section, we examine the important characteristic of neighboring chaotic orbits to see how rapidly they separate each other.

This separation is quantified by using the concept of Lyapunov exponents [Oseledec, 1968]. In general, the Lyapunov exponents can only be found by computations using a monitored long-term time series.

In system (2), Lyapunov exponents can be calculated rigorously by using a method proposed in [MÏller, 1995]. Nevertheless, by using the efficient algorithm given in [Wolf, 1986], we have found three Lyapunov exponents as follows:

$$\lambda_1 = 0.38\,, \quad \lambda_2 = 0.23\,, \quad \lambda_3 = -1.26\,,$$

which quantify the rapidity of separation of orbits inside the attractor.

A typical situation for a continuous-time three-dimensional autonomous chaotic system *with a continuous vector field* is that there are three Lyapunov exponents, ℓ_i, satisfying $\ell_1 > 0$, $\ell_2 = 0$, $\ell_3 < 0$ and $\ell_1 + \ell_2 + \ell_3 < 0$. However, it is interesting to see that this is not the case for system (2). This is because system (2) has a *discontinuous vector field* due to the signum functions on its right-hand side, therefore it may not possess some familiar features of the continuous or smooth dynamical systems. This interesting phenomenon deserves special attention

and detailed analysis, which will be further investigated in the near future.

Moreover, for system (2), its Lyapunov dimension (see e.g. [Kaplan & York, 1979]), is defined as follows:

$$d_L = j + \frac{\sum_{i=1}^{i=j} \ell_i}{|\ell_{j+1}|}$$

with $\ell_1 \geq \cdots \geq \ell_n$, where j is the largest integer such that $\sum_{i=1}^{i=j} \ell_i \geq 0$ and $\sum_{i=1}^{i=j+1} \ell_i < 0$.

In our case, the Lyapunov dimension is

$$d_L = 2 + \frac{\lambda_1 + \lambda_2}{|\lambda_3|}\,.$$

Therefore, system (2) has a fractal dimension $d_L \approx 2 + (0.61/1.26) \approx 2.48$.

3.3. *Bifurcation diagrams and some phase portraits*

For system (2), a typical period-doubling route to chaos is observed, as shown in Fig. 6. This figure gives a bifurcation diagram for the system with the parameters fixed by Eq. (9) and a is varied as the bifurcation parameter: $a \in [1.13, 1.18]$. In this diagram, asymptotic values of $x(t)$ are plotted as a function of a.

As the parameter a is increased, the period-2 behavior bifurcates to a period-4 cycle, after which period-doubling bifurcations continue. This culminates in a Feigenbaum cascade of period-doubling bifurcations leading to a chaotic region beginning at $a = 1.155\ldots$ approximately. The chaotic region contains trajectories that are completely nonperiodic, as well as periodic orbits of arbitrary

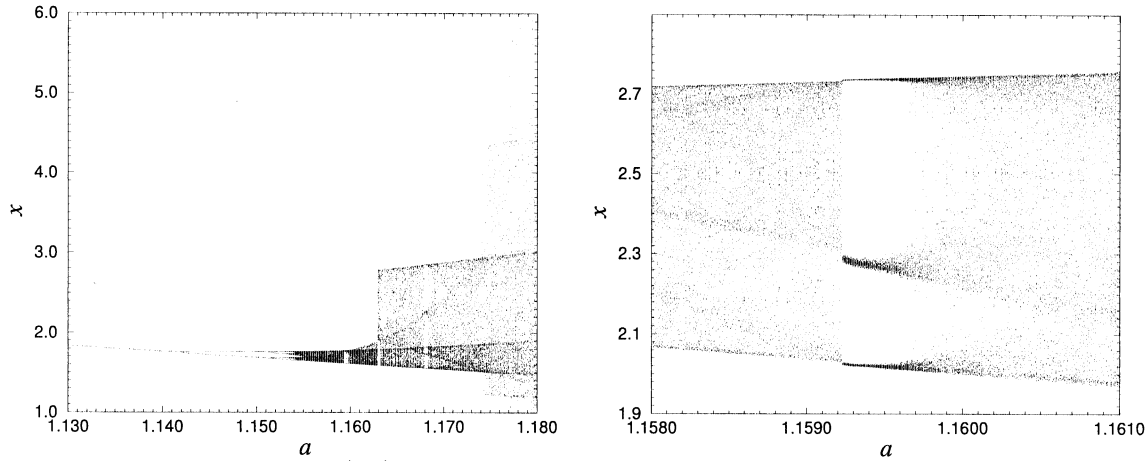

(a) (b)

Fig. 6. (a) One-parameter bifurcation diagram of system (2) with respect to the control parameter a, while the other parameters are fixed by Eq. (9); (b) magnification of the first diagram: between $a = 1.158$ and $a = 1.161$.

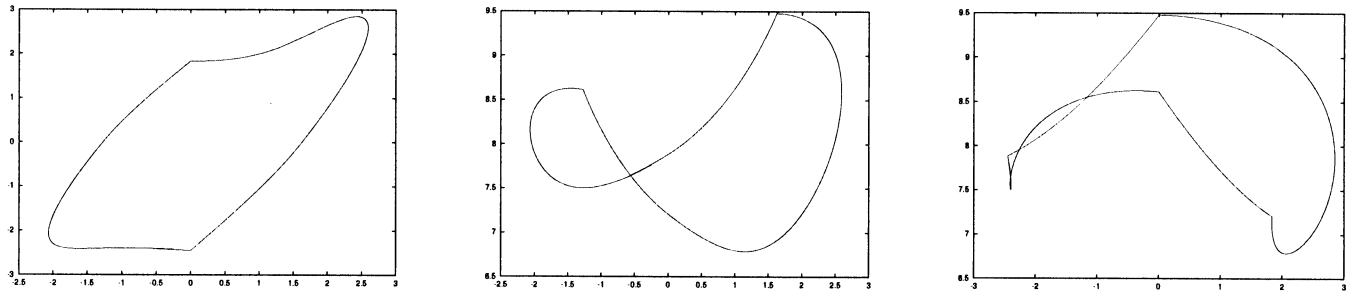

(a) (b) (c)

Fig. 7. A nonsymmetric stable period-1 orbit, obtained with $a = 1.13$.

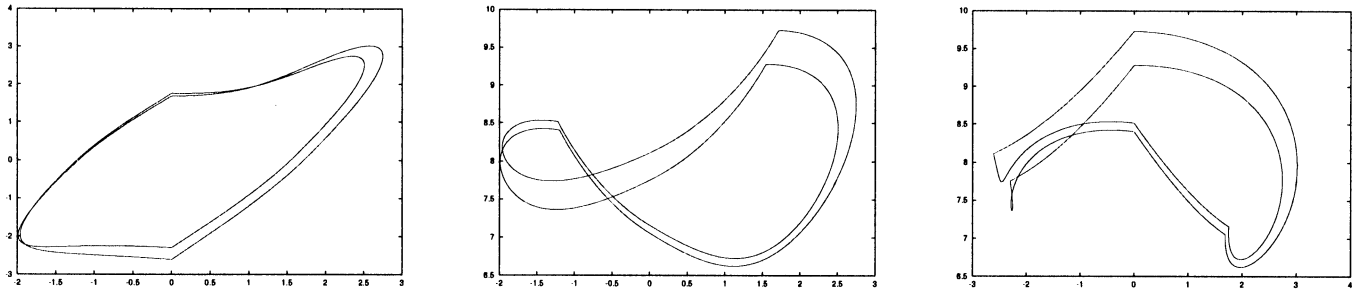

(a) (b) (c)

Fig. 8. A nonsymmetric stable period-2 orbit, obtained with $a = 1.15$.

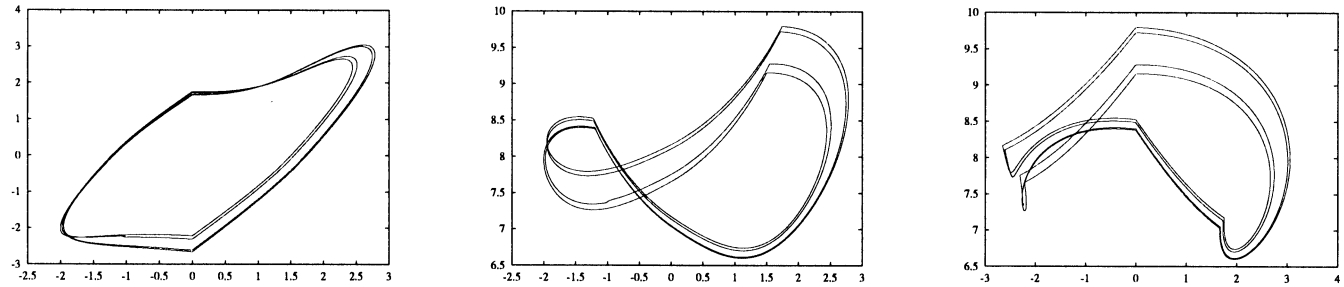

(a) (b) (c)

Fig. 9. A nonsymmetric stable period-4 orbit, obtained with $a = 1.153$.

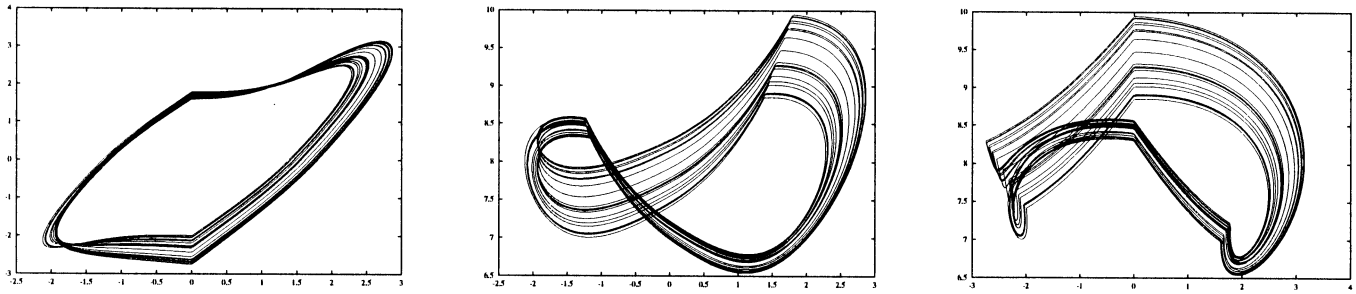

(a) (b) (c)

Fig. 10. A nonsymmetric quasi-periodic orbit, obtained with $a = 1.16$ and initial conditions $X_0(-1.0,\ 0.1,\ 10.0)$.

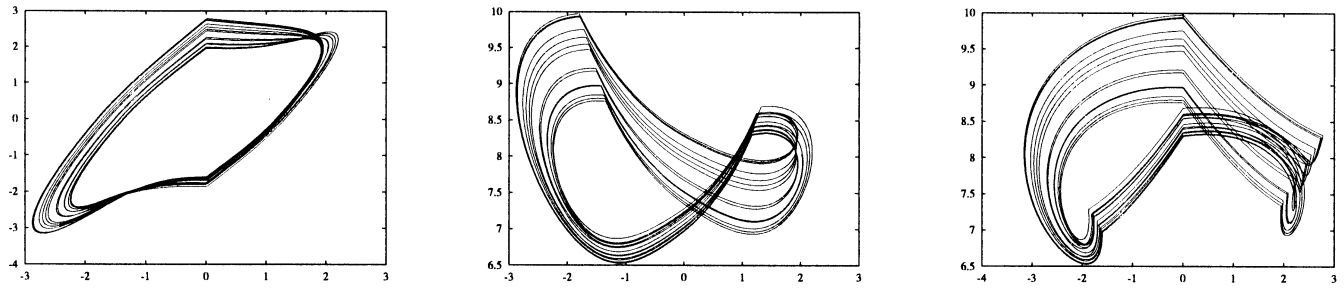

(a) (b) (c)

Fig. 11. The "symmetric" orbit of the nonsymmetric quasi-periodic orbit, of the previous picture (the same parameter values as the previous figure), corresponding to the initial conditions $X_0'(1.0,\ -0.1,\ 10.0)$.

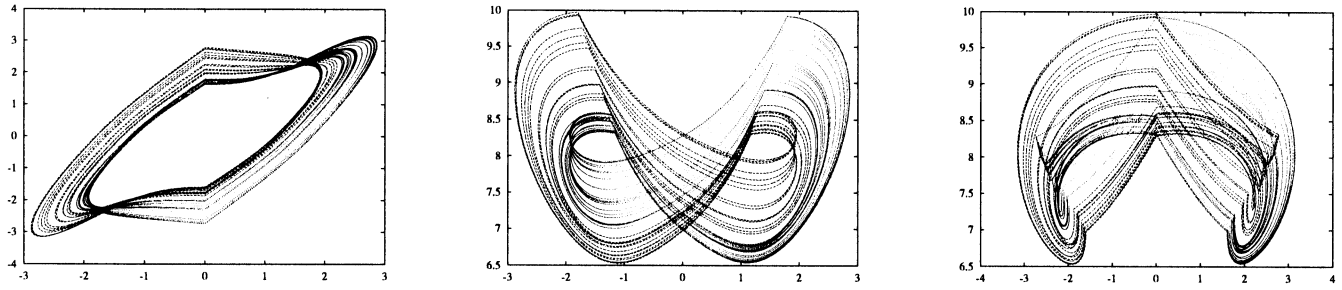

(a) (b) (c)

Fig. 12. Orbits of both previous pictures (Figs. 10 and 11) plotted together, with $a = 1.16$.

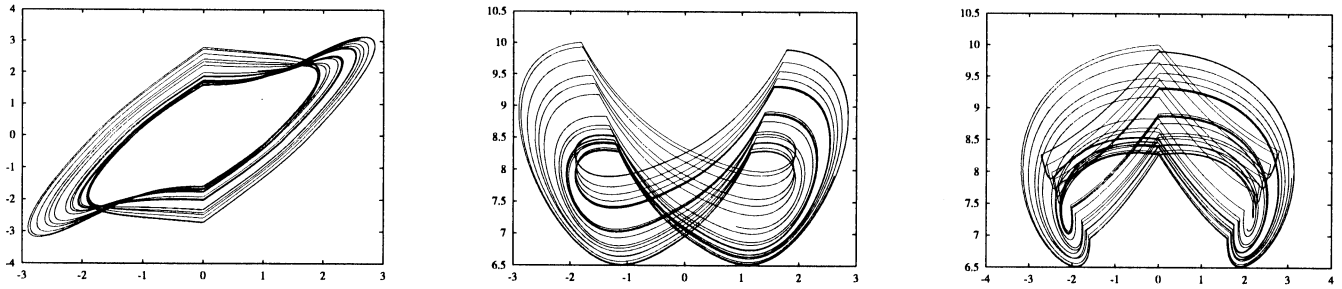

(a) (b) (c)

Fig. 13. A "symmetric" (chaotic) orbit, obtained with $a = 1.164$ and initial conditions $X_0(-1.0, 0.1, 10.0)$.

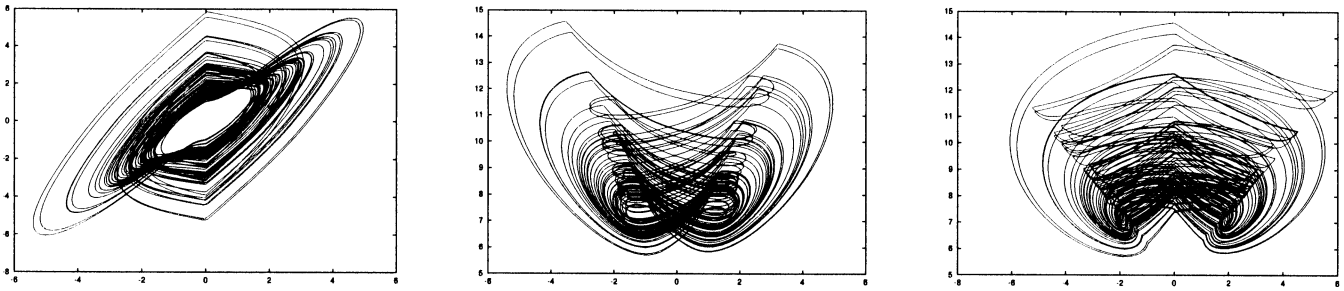

(a) (b) (c)

Fig. 14. A "symmetric" (chaotic) attractor, obtained with $a = 1.18$.

periods. In some cases, these orbits may be non-symmetric; their "symmetric" orbits coexist due to the invariance of the system under the transform $(x, y, z) \to (-x, -y, z)$; and as a increases, these attractors grow slightly in size, become more complex, and then they are merged leading to the formation of a "symmetric" attractor (Figs. 7–14).

Figures 7–14 illustrate the cascade of bifurcations found for the set of parameters specified by Eq. (9), using again a as the control parameter. In these figures, the one on the left is the x–y plane projection of the solution, the central one is its x–z plane projection, and the one on the right is the y–z plane projection.

4. Conclusion with Perspective

We have reported the finding of a new chaotic attractor in a piecewise-linear continuous-time three-dimensional autonomous system obtained by a

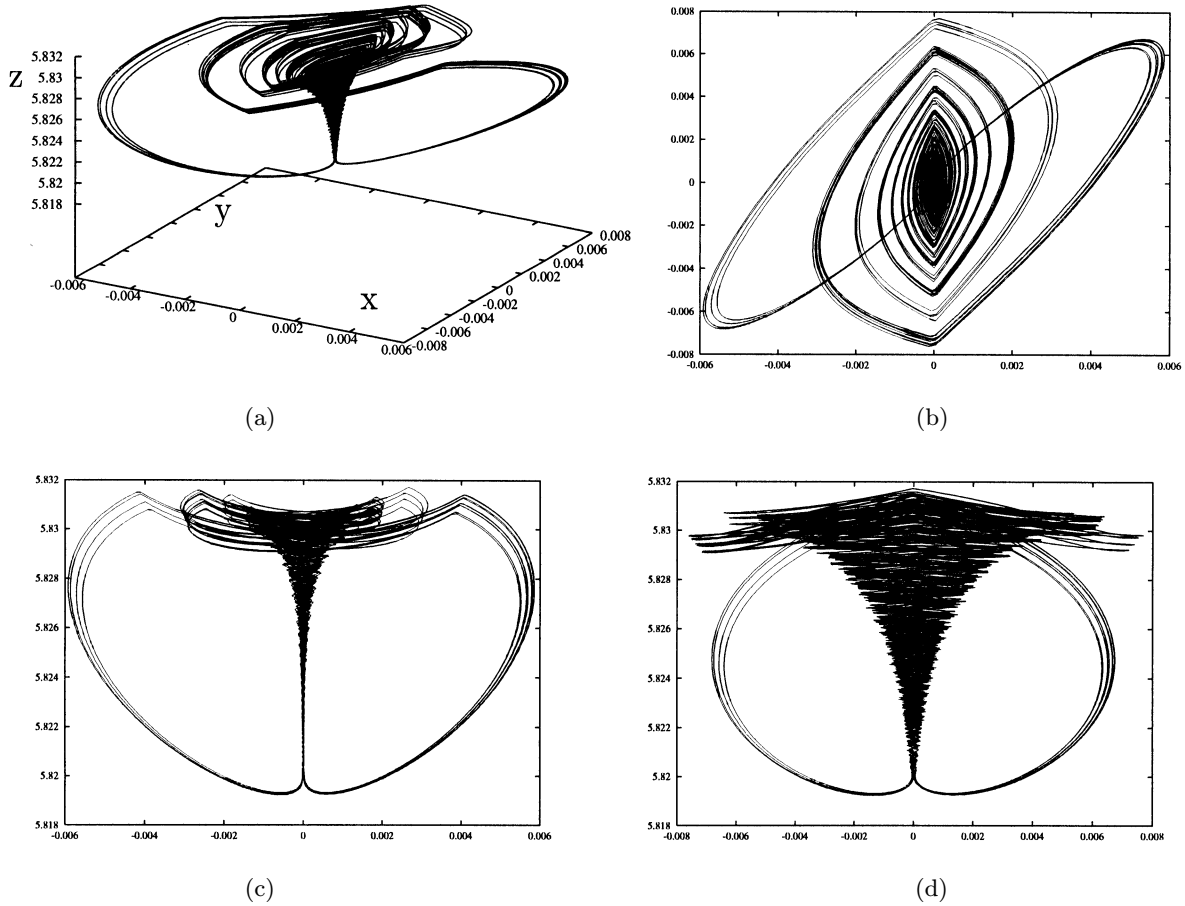

Fig. 15. Another "symmetric" chaotic attractor found from system (2), with parameters $a = 1.18$, $b = 0.0001$, $c = 7.0$ and $q = 0.1$: (a) Three-dimensional view, projections on (b) x–y plane, (c) x–z plane, (d) y–z plane.

direct modification of the existing Chen's system. We have then briefly discussed its complex chaotic dynamics, which turns out to be quite rich, as also shown in Fig. 15 for parameters that were not studied in the paper above. More detailed analysis for such phenomena will be provided in the near future.

Acknowledgments

M. A. Aziz-Alaoui is grateful for the support from the Department of International Relations (SRI) of Le Havre University.

G. Chen acknowledges the support from the US Army Research Office under the Grant DAAG55-98-1-0198 and the Hong Kong CERG Grant 9040565.

References

Aziz-Alaoui, M. A. [1999] "Differential equations with multispiral attractors," *Int. J. Bifurcation and Chaos* **9**(6), 1009–1039.

Aziz-Alaoui, M. A. [2001] "Yet a new piecewise-linear chaotic system," *Sci. Lett.* **3**(1).

Baghious, E. H. & Jarry, P. [1993] "Lorenz attractor from differential equations with piecewise-linear terms," *Int. J. Bifurcation and Chaos* **3**(1), 201–210.

Chen, G. [1997] "Control and anticontrol of chaos," *Proc. 1st Int. Conf. Control of Oscillations and Chaos*, St. Pertersburg, Russia, August 27–29, 1997, pp. 181–186.

Chen, G. & Lai, D. [1998] "Feedback anticontrol of discrete chaos," *Int. J. Bifurcation and Chaos* **8**, 1585–1590.

Chen, G. & Ueta, T. [1999] "Yet another chaotic attractor," *Int. J. Bifurcation and Chaos* **9**(7), 1465–1466.

Chua, L. O. [1990] "Canonical realisation of Chua's circuit family," *IEEE Trans. Circuits Syst.* **37**, 885–902.

Cooley, J. W. & Tukey, J. W. [1965] "An algorithm for the machine calculations of complex Fourier series," *Math. Comput.* **19**, 297–301.

Grassberger, P. & Procaccia, I. [1983] "Characterization of strange attractors," *Phys. Rev. Lett.* **50**(5), 346–349.

Kaplan, J. L. & York, Y. A. [1979] "A regime observed in a fluid flow model of Lorenz," *Commun. Math. Phys.* **67**, 93–108.

Lorenz, E. N. [1961] "Deterministic nonperiodic flow," *J. Atoms. Sci.* **20**, 130–141.

Lü, J., Chen, G. & Zhang, S. [2002] "Dynamical analysis of a new chaotic attractor," *Int. J. Bifurcation and Chaos* **12**(5), in press.

MÏller, P. C. [1995] "Calculation of Lyapunov exponents for dynamic systems with discontinuities," *Chaos Solit. Fract.* **5**, 1671–1681.

Oseledec, V. I. [1968] "A multiplicative ergodic theorem: Lyapunov characteristic numbers for dynamical systems," *Trans. Moscow Math. Soc.* **19**, 197–231.

Sparrow, C. [1982] *The Lorenz Equations*: *Bifurcations*, *Chaos and Strange Attractors*, *Applied Mathematical Science*, Vol. 41 (Springer-Verlag, NY).

Tang, K. S., Man, K. F., Zhong, C. Q. & Chen, G. [2001] "Generating chaos via $x|x|$," *IEEE Trans. Circuit Syst. I — Fundamental Th. Appl.* **48**(5), 636–641.

Tokunaga, R., Komuro, M., Matsumoto, T. & Chua, L. O. [1989] "Lorenz attractor from an electrical circuit with uncoupled piecewise-linear continuous resistors," *Int. J. C. T. A.* **17**(1), 71–85.

Wang, X. & Chen, G. [1999] "On feedback anticontrol of discrete chaos," *Int. J. Bifurcation and Chaos* **9**(7), 1435–1441.

Wang, X. & Chen, G. [2000] "Chaotification via arbitrarily small feedback controls: Theory, method, and applications," *Int. J. Bifurcation and Chaos* **10**(3), 549–570.

Wolf, A. [1986] "Quantifying chaos with Lyapunov exponents," in *Chaos*, ed. Holden, A. V. (Manchester University Press, Manchester, UK), pp. 273–290.